# Relic neutrino decay solution to the excess radio background

Journal of Cosmology and Astroparticle Physics
An IOP and SISSA journal

Received: *January 11, 2024*
Accepted: *February 26, 2024*
Published: *April 16, 2024*

# Relic neutrino decay solution to the excess radio background

**P.S. Bhupal Dev**,[a] **Pasquale Di Bari**,[b,*] **Ivan Martínez-Soler**[c] **and Rishav Roshan**[b]

[a] *Department of Physics and McDonnell Center for the Space Sciences, Washington University, St. Louis, Missouri 63130, U.S.A.*
[b] *School of Physics and Astronomy, University of Southampton, Southampton, SO17 1BJ, U.K.*
[c] *Institute for Particle Physics Phenomenology, Department of Physics, Durham University, Durham DH1 3LE, U.K.*

*E-mail:* bdev@wustl.edu, p.di-bari@soton.ac.uk, ivan.j.martinez-soler@durham.ac.uk, r.roshan@soton.ac.uk

Abstract: The excess radio background detected by ARCADE 2 represents a puzzle within the standard cosmological model. There is no clear viable astrophysical solution, and therefore, it might indicate the presence of new physics. Radiative decays of a relic neutrino $\nu_i$ (either $i = 1$, or $i = 2$, or $i = 3$) into a sterile neutrino $\nu_{\rm s}$, assumed to be quasi-degenerate, provide a solution that currently evades all constraints posed by different cosmological observations and reproduces very well the ARCADE 2 data. We find a very good fit to the ARCADE 2 data with best fit values $\tau_i = 1.46 \times 10^{21}\,{\rm s}$ and $\Delta m_i = 4.0 \times 10^{-5}\,{\rm eV}$, where $\tau_i$ is the lifetime and $\Delta m_i$ is the mass difference between the decaying active neutrino and the sterile neutrino. On the other hand, if relic neutrino decays do not explain ARCADE 2 data, then these place a stringent constraint $\Delta m_i^{3/2}\tau_i \gtrsim 2 \times 10^{14}\,{\rm eV}^{3/2}\,{\rm s}$ in the range $1.4 \times 10^{-5}\,{\rm eV} < \Delta m_i < 2.5 \times 10^{-4}\,{\rm eV}$. The solution also predicts a stronger 21 cm absorption global signal than the predicted one from the ΛCDM model, with a contrast brightness temperature $T_{21} = -238^{+21}_{-20}\,{\rm mK}$ (99% C.L.) at redshift $z \simeq 17$. This is in mild tension with the even stronger signal found by the EDGES collaboration, $T_{21} = -500^{+200}_{-500}\,{\rm mK}$, suggesting that this might have been overestimated, possibly receiving a contribution from some unidentified foreground source.

Keywords: CMBR theory, cosmological neutrinos, neutrino properties

ArXiv ePrint: 2312.03082

*Corresponding author.



https://doi.org/10.1088/1475-7516/2024/04/046

JCAP04(2024)046

## Contents


**1 Introduction** 1

**2 Effective temperature of non-thermal radiation** 5

**3 Fitting the ARCADE 2 excess radio background** 6

**4 Predicting the 21 cm cosmological global absorption signal** 11

**5 On dark matter decays/de-excitations as alternative explanation** 14

**6 Final remarks** 16


## 1 Introduction

The cosmological puzzles, in particular dark matter and matter-antimatter asymmetry of the universe, and the discovery of neutrino masses in neutrino oscillation experiments, clearly indicate the existence of new physics. However, we are still far from understanding the new framework that can accommodate them. Most of the efforts have so far relied on collider physics, dark matter searches and low-energy neutrino experiments. However, the rich variety of cosmological observations provides other interesting alternative ways to understand how new physics could manifest itself and these should not be overlooked or undermined.

The Absolute Radiometer for Cosmology, Astrophysics and Diffuse Emission (ARCADE 2) is a balloon-borne instrument that has measured the absolute temperature of the sky in the 3–90 GHz radio frequency range [1]. A data analysis has found an extragalactic excess, in addition to the cosmic microwave background (CMB), at the low edge of the frequency range, approximately between 3 and 8 GHz. The excess fades away at higher frequencies, so that results consistent with the CMB background spectrum measured by the Far Infrared Absolute Spectrophotometer (FIRAS) instrument [2] are recovered in the far infrared frequency range 60–600 GHz. Moreover, when the ARCADE 2 data are combined with those from previous measurements at lower frequencies, in the range 22 MHz–1.42 GHz, it is found that a background power law spectrum with spectral index $\beta = -2.60 \pm 0.04$ describes well all data [1].

More recently, a study of the low frequency all-sky maps from the Long Wavelength Array (LWA) measured the diffuse radio background between 40 and 80 MHz, also finding an excess [3]. In combination with the ARCADE 2 data, this analysis confirms a background power law spectrum with spectral index $\beta = -2.58 \pm 0.05$. This excess radio background cannot be explained by known population of sources since they give a contribution to the effective temperature that is 3–10 times smaller than the measured one [4]. Part of the excess radio background is due to galactic synchrotron radiation but this galactic contamination is significantly below the background [5]. Recently, low-redshift populations of discrete extragalactic radio sources have been also excluded by angular cross-correlating data of the



JCAP04(2024)046

diffuse radio sky with matter tracers at different redshifts provided by galaxy catalogs and CMB lensing [6]. More exotic astrophysical explanations of the excess radio background have proposed an origin from unknown radio source counts at high redshift, such as supermassive black holes and star forming galaxies. However, a study of the diffuse extragalactic radio emission at 1.75 GHz using the Australia Telescope Compact Array (ATCA), constrains the contribution to the background of extended sources with angular size as large as 2 arcmin [7]. These and other observations place a strong upper limit on the anisotropy of the excess radio background that is, therefore, extremely smooth [8]. This represents a strong constraint for an astrophysical origin. For this reason, many explanations in terms of new physics have been proposed such as: WIMP annihilations or decays in extra-galactic halos [9]; synchrotron radiation emitted by the electrons produced by the late decays of a metastable particle in a magnetic field [10]; dark photons, produced by dark matter decays, oscillating into ordinary photons [11]; superconducting cosmic strings [12, 13]; soft photon emission from accreting primordial black holes [14]; radiative decay of relic neutrinos into sterile neutrinos [15]. Also in this case the smoothness of the background strongly constrains some of these solutions, in particular those relating the origin of the excess radio background to dark matter.[1] Some of these explanations are also constrained by other cosmological observations [16, 17] but additional data will be necessary to draw firm conclusions. In this respect, it is interesting that more measurements will come both from CMB experiments with a smaller low frequency threshold than FIRAS, such as the Primordial Inflation Explorer (PIXIE) [18] or its more advanced versions Super-PIXIE [19] and VOYAGE 2050 [20], that will measure deviations of the CMB spectrum from thermal down to 30 GHz, and from radio interferometers such as the Tenerife Microwave Spectrometer (TMS) that will cover the 10–20 GHz frequency range [21, 22].

An important point is that even if just a small fraction of the excess radio background detected at the present time has to be ascribed to redshifted radiation produced at high redshifts (at least $z \gtrsim 20$), this would produce a sizeable deviation of the cosmological 21 cm global absorption signal from the standard prediction [23], where the only contribution comes from the CMB radiation [24]. For example, even if only 0.1% of the background has a high redshift origin, this would be enough to produce a detectable effect [23]. Recently, it has been pointed out that a soft photon heating effect, due to inverse bremsstrahlung absorption by the background electrons, should also be taken into account [25]. This can strongly reduce the absorption 21 cm global signal expected from the observed excess radio background and it has been specifically shown to be important in decaying particle scenarios, as the one we will consider. In any case some deviation from the standard prediction is expected.

It is then intriguing that the Experiment to Detect the Reionization Step (EDGES) collaboration has indeed claimed evidence of a 21 cm global absorption signal falling approximately in the expected interval of redshifts within standard cosmology but about twice stronger [26]. It has to be said that such a claim has not yet been confirmed by other experiments. Moreover, concerns related to various possible sources of underestimated systematic uncertainties have been discussed such as ionospheric effects [27] and inhomogeneities of the ground below the EDGES antenna [28]. In addition, the Shaped Antenna measurement of

[1] We refer to dark matter as the dominant component of dark matter, cold or warm.



JCAP04(2024)046

the Background RAdio Spectrum (SARAS 3) experiment collaboration has found no evidence of the absorption signal, rebutting the EDGES claim [29]. Both concerns and the rebuttal have been addressed respectively in [30–32]. It is anyway important that a few experiments, in addition to SARAS 3, are underway to test the EDGES claimed anomaly in next years, including: the Large-aperture Experiment to Detect the Dark Ages (LEDA) [33], the Mapper of the IGM Spin Temperature (MIST) [34], Probing Radio Intensity at High-Z from Marion (PRIZM) [35], the Radio Experiment for the Analysis of Cosmic Hydrogen (REACH) [36], and Hydrogen Epoch of Reionization Array (HERA) [37]. Moreover, space and lunar-based global 21 cm experiments, such as Discovering Sky at the Longest wavelength (DSL) [38], the Lunar Surface Electromagnetic Experiment (LuSEE) [39] and Probing ReionizATion of the Universe using Signal from Hydrogen (PRATUSH) [40], are also planned to start operating in the next few years. These will be able to circumvent observational systematics associated with the ionosphere and human-made radio frequency interference.

The anomalous absorption 21 cm signal claimed by EDGES has stimulated a variety of different proposals for its explanation. The signal can be expressed in terms of the 21 cm brightness temperature $T_{21}(z)$. At redshifts $z \sim 10$–$25$ this is approximately proportional to $1 - T_\gamma(\nu_{21}^{\rm rest}, z)/T_{\rm gas}(\nu_{21}^{\rm rest}, z)$, where $T_\gamma(\nu_{21}^{\rm rest}, z)$ is the effective temperature of radiation and $T_{\rm gas}(\nu_{21}^{\rm rest}, z)$ is the temperature of the gas at redshift $z$ at the 21 cm rest frequency $\nu_{21}^{\rm rest} = 1420\text{MHz}$. This corresponds today to a redshifted (observed) frequency $\nu_{21}(z) = \nu_{21}^{\rm rest}/(1+z)$. Since in this range of redshifts one has $T_{\rm gas}(z) < T_\gamma(z)$, then $T_{21}(z) < 0$, corresponding to an absorption signal. The EDGES collaboration has claimed evidence of an absorption signal just in the expected range of redshifts and with a minimum at $z_E \simeq 17.2$, corresponding to $\nu_{21}(z_E) \simeq 78\,\text{MHz}$ but with a minimum value of $T_{21}$ about 2.5 times lower than expected in $\Lambda$CDM. Explanations of this anomalous discrepancy can be divided into two categories: (i) the absorption signal is enhanced by cooling the gas temperature compared to the standard case; (ii) the radiation effective temperature is higher than in the standard case, where it is given simply by the CMB temperature, implying the presence of some extra radiation in addition to relic thermal radiation that could also explain the excess radio background.

In the first category, solutions necessarily rely on new physics. For example, it was proposed that gas is made colder by the interactions with the dark matter [41]. Different constraints single out a solution where the gas should interact with millicharged particles that give only a subpercent fraction of the total dark matter energy density [42]. In the second category one can think of astrophysical solutions relying on the existence of unknown astrophysical sources of radiation in the radio frequencies. For example, it has been proposed that accretion onto the first intermediate-mass black holes between $z \simeq 30$ and $z \simeq 16$ can explain the EDGES anomaly [43]. However, these kind of solutions necessarily rely on not so well established mechanisms that prevent X-ray emission with consequent heating of the intergalactic medium that could change the reionization history incompatibly with the CMB anisotropy observations. Because of the challenges encountered by astrophysical solutions able to explain the EDGES anomaly with the presence of extra radiation, also many solutions relying on new physics have been proposed, such as: decay or de-excitations of some fraction of dark matter [44]; resonant oscillations of dark photons into regular photons [45]; radiative decay of relic neutrinos into sterile neutrinos [15]; superconducting cosmic strings [12, 13];



JCAP04(2024)046

conversion of mirror photons into standard photons [46]. In most cases these have also been discussed in combination with an explanation of the ARCADE 2 excess radio background. In this paper we revisit the case of relic neutrino radiative decays since it currently represents an attractive option to produce extra non-thermal radiation for a few reasons:

(i) It provides a solution to the ARCADE 2 excess and potentially also to the EDGES anomaly.

(ii) It is minimal since it involves essentially only two parameters: the lifetime of neutrinos and the mass difference between the relic neutrinos and the invisible particle into which it decays. We will consider the case of a sterile neutrino as originally proposed in [15] but it should be clear that the discussion might be extended to other cases.

(iii) The relic neutrino abundance can be assumed to be the standard one predicted by the ΛCDM model and it is therefore fixed.

(iv) Since neutrinos are fermions, their clustering is very limited, especially for current neutrino mass bound $m_i \lesssim 0.1\,\mathrm{eV}$, compared to cold dark matter [47, 48]. Therefore, it predicts a very smooth excess radio background, as supported by the observations, and so it does not suffer the tension of models where the excess radio background is related to the dark matter abundance.

We will show that the spectrum predicted by this solution fits very well the ARCADE 2 data and has some very definite features that makes it distinguishable from other models, like for example the single power law model proposed to explain also LWA data in a combined way. In particular, the spectrum presents a transition between two different power laws and has a sharp end point. It makes a very precise prediction for the brightness contrast temperature $T_{21}$ in the 21 cm absorption global signal. As we will see this is in mild tension with the EDGES anomaly since it predicts a weaker signal, though still with a sizeable observable deviation from the standard case. We will also comment on the fact that the same kind of spectrum can be obtained from dark matter decays/de-excitations but only for masses of dark matter below 10 keV.

The paper is structured as follows. In section 2 we briefly review the derivation of the effective temperature of non-thermal radiation produced from radiative relic neutrino decays. In section 3 we specialise it to zero redshift to fit the excess radio background data from ARCADE 2. We find the best fit and the 99% C.L. allowed region in the plane $\Delta m_1$ vs. $\tau_1$. In section 4 we consider the 21 cm cosmological absorption signal claimed by EDGES and also in this case we specialise the general formula and find the 99% C.L. allowed region noticing that there is a tension with the ARCADE 2 allowed region. We also derive the prediction on the brightness contrast temperature $T_{21}$ from ARCADE 2 data. In section 5 we discuss the case of dark matter de-excitations, introducing a third parameter given by the dark matter mass and showing how, for dark matter masses much higher than about 10 keV, only the EDGES anomaly can be explained, not the ARCADE 2 excess radio background data. Finally, in section 6 we draw our conclusions making some final remarks.



JCAP04(2024)046

## 2 Effective temperature of non-thermal radiation

Let us derive the effective temperature of non-thermal photons produced from the radiative decays of relic neutrinos. For definiteness, we will refer to the decay of the lightest neutrino $\nu_1$, since this presents different attractive features compared to the decays of the two heavier neutrinos. However, our results can also be extended to that case. We will consider radiative two body decays into sterile neutrinos with mass $m_{\rm s}$. The lightest active neutrino and the sterile neutrino are assumed to be quasi-degenerate, so that $\Delta m_1 \equiv m_1 - m_{\rm s} \ll m_1$. We also assume that the lightest neutrinos decay non-relativistically in a way that at the production photons from decays are approximately monochromatic. In this case the *specific intensity* at redshift $z$ of the non-thermal photons of energy $E \leq \Delta m_1$ is given by[2]

$$I_{\gamma_{\rm nth}}(E,z) = \frac{1}{4\pi}\frac{d\varepsilon_{\gamma_{\rm nth}}}{dE} = \frac{n^{\infty}_{\nu_1}(z)}{4\,\pi}\frac{e^{-\frac{t(a_{\rm D})}{\tau_1}}}{H(a_{\rm D})\,\tau_1}\,, \tag{2.1}$$

where $\tau_1$ is the active neutrino lifetime, $\varepsilon_{\gamma_{\rm nth}}$ is the energy density of the non-thermal radiation, $H(a_{\rm D})$ and $t(a_{\rm D})$ are, respectively, the expansion rate and the age of the universe calculated at the time of decay of the relic neutrinos that produced photons with energy $E$ at redshift $z$, corresponding to a redshift $z_{\rm D} \equiv a_{\rm D}^{-1} - 1$ and scale factor $a_{\rm D} = (E/\Delta m_1)\,a \leq a$, and

$$n^{\infty}_{\nu_1}(z) = \frac{6}{11}\frac{\zeta(3)}{\pi^2}\,T^3(z) \tag{2.2}$$

is the relic neutrino number density at $z$ in the standard stable neutrino case ($T$ is the standard relic photon temperature).

The expansion rate at the decay, $H(a_{\rm D})$, can be calculated in the $\Lambda$CDM model as

$$H(a_{\rm D}) = H_0\,\sqrt{\Omega_{\rm M0}\,a_{\rm D}^{-3} + \Omega_{\Lambda 0}} = H_0\,\sqrt{\Omega_{M0}}\,a_{\rm D}^{-\frac{3}{2}}\left(1 + \frac{a_{\rm D}^3}{a_{\rm eq}^3}\right)^{\frac{1}{2}}\,, \tag{2.3}$$

where $a_{\rm eq} \equiv (\Omega_{M0}/\Omega_{\Lambda 0})^{1/3} \simeq 0.77$, $\Omega_{M0} \simeq 0.3111$, $H_0 \simeq t_0^{-1}$ and $t_0 \simeq 13.8\,{\rm Gyr} \simeq 4.35 \times 10^{17}\,{\rm s}$ [50].[3] An analytical expression for the age of the universe at the decay, $t(a_{\rm D})$, can also be found within the $\Lambda$CDM model [52]:

$$t(a_{\rm D}) = \frac{2}{3}\frac{H_0^{-1}}{\sqrt{\Omega_{\Lambda 0}}}\,\ln\left[\sqrt{\left(\frac{a_{\rm D}}{a_{\rm eq}}\right)^3} + \sqrt{1 + \left(\frac{a_{\rm D}}{a_{\rm eq}}\right)^3}\right]\,. \tag{2.4}$$

The specific intensity from non-thermal photons produced by relic neutrino decays would give, at the frequency $\nu$ at redshift $z$, an excess with respect to the specific intensity of the thermal radiation that is simply given by

$$I_{\rm th}(E,z) \equiv \frac{d\mathcal{F}_E^{\gamma_{\rm th}}}{dA\,dt\,dE\,d\Omega} = \frac{1}{4\pi}\frac{d\varepsilon_{\gamma_{\rm th}}}{dE} = \frac{E^3}{4\,\pi^3}\,[e^{E/T(z)} - 1]^{-1}\,. \tag{2.5}$$

[2] This expression further generalises the expression given in [15] that extended the expression given in [49] for the case $z = 0$.

[3] We can neglect statistical errors on cosmological parameters for the determination of the best fit value for $\tau_1$ (as a function of $\Delta m_1$). We just notice that taking $H_0 = t_0^{-1} = 71\,{\rm km\,s^{-1}\,Mpc^{-1}}$ corresponds to a kind of average value between the CMB determination $H_0 \simeq 67\,{\rm km\,s^{-1}\,Mpc^{-1}}$ [50] and the SH0ES determination from SNIa $H_0 \simeq 73\,{\rm km\,s^{-1}\,Mpc^{-1}}$ [51]. This uncertainty on $H_0$, the so-called Hubble tension, is also negligible for the determination of $\tau_1$ with current measurements of the excess radio background.



JCAP04(2024)046

In the Rayleigh-Jeans tail, for $E = h\nu \ll T(z)$, the specific intensity depends linearly on temperature:

$$I_{\rm th}(E,z) = \frac{E^3}{4\,\pi^3}\,[e^{E/T(z)}-1]^{-1} \overset{E\ll T(z)}{\longrightarrow} \frac{1}{4\pi^3}\,T(z)\,E^2\,. \tag{2.6}$$

For some generic non-thermal radiation, it is customary to introduce an *effective photon temperature* $T_{\gamma_{\rm nth}}(E,z)$ defined as the temperature corresponding to a thermal radiation with the same specific intensity at the given arbitrary frequency $\nu$ and redshift $z$, explicitly:

$$T_{\gamma_{\rm nth}}(E,z) = E\,\ln^{-1}\left(1+\frac{E^3}{4\,\pi^3\,I_{\gamma_{\rm nth}}(E,z)}\right). \tag{2.7}$$

Again, in the low frequency limit, for $E \ll T_\gamma$, one has a simple linear relation between the effective temperature and the specific intensity:

$$T_{\gamma_{\rm nth}}(E,z) \simeq \frac{4\pi^3}{E^2}\,I_{\gamma_{\rm nth}}(E,z)\,. \tag{2.8}$$

This gives us a general formula valid at any redshift. In the case of ARCADE 2 the measurements are made at zero redshift. In the case of EDGES the 'detection' occurs at $z \sim z_E$ and it is seen today as a (redshifted) absorption feature.

## 3 Fitting the ARCADE 2 excess radio background

Let us see how the expression (2.1) can describe the ARCADE 2 measurements of the excess radio background temperature, defined as $T_{\rm ERB} \equiv T_{\gamma 0} - T_0$, shown in table 1. Notice that the ARCADE 2 experiment found $T_0 = (2.729 \pm 0.004)\,{\rm K}$, in very good agreement with the FIRAS measurement.

In the case of ARCADE 2, the measurements are made at $z = 0$, so that, specialising eq. (2.1) at $z = 0$, the predicted specific intensity of the non-thermal component produced by the relic neutrino decays is given by

$$I_{\gamma_{\rm nth}}(E,0) = \frac{n^{\infty}_{\nu_1}(0)}{4\,\pi}\,\frac{e^{-\frac{t(a_{\rm D})}{\tau_1}}}{H(a_{\rm D})\,\tau_1}\,. \tag{3.1}$$

Since we are in the regime $E \ll T_\gamma$, we can simply use eq. (2.8) to calculate the predicted effective temperature of the excess radio background from relic neutrino decays. Moreover, we will consider the case $\tau_1 \gg t_0$,[4] so that the exponential can be safely approximated by unity and in the end we obtain:

$$T_{\gamma_{\rm nth}}(E,0) \simeq \frac{6\,\zeta(3)}{11\,\sqrt{\Omega_{\rm M0}}}\,\frac{T_0^3}{E^{1/2}\,\Delta m_1^{3/2}}\,\frac{t_0}{\tau_1}\left(1+\frac{a_{\rm D}^3}{a_{\rm eq}^3}\right)^{-\frac{1}{2}}\,. \tag{3.2}$$

In table 1 we show the effective temperature of the excess radio background measured by ARCADE 2 at 9 different frequencies. As one can see from the table, only the first four measurements indicate some excess with non-negligible statistical significance. The fifth

[4] We will comment in the conclusions on the existence of the solution for $\tau_1 \ll t_0$ reported in [15].



JCAP04(2024)046

| $i$ | $\nu_i$ (GHz) | $E_i$ ($10^{-5}$ eV) | $T^i_{\gamma 0}$ (K) | $\overline{T}^i_{\rm ERB}$ (mK) | $\delta T^i_{\rm ERB}$ (mK) |
|---|---|---|---|---|---|
| 1 | 3.20 | 1.36 | 2.792 | 63 | 10 |
| 2 | 3.41 | 1.41 | 2.771 | 42 | 9 |
| 3 | 7.97 | 3.30 | 2.765 | 36 | 14 |
| 4 | 8.33 | 3.44 | 2.741 | 12 | 16 |
| 5 | 9.72 | 4.02 | 2.732 | 3 | 6 |
| 6 | 10.49 | 4.34 | 2.732 | 3 | 6 |
| 7 | 29.5 | 12.2 | 2.529 | −200 | 155 |
| 8 | 31 | 12.82 | 2.573 | −156 | 76 |
| 9 | 90 | 37.2 | 2.706 | −23 | 19 |

**Table 1.** ARCADE 2 measurements of the excess radio background effective temperature [1].

and sixth points seem to be compatible with zero within the errors. The other three points, seventh to ninth in the table, have very large errors and/or give a negative result. As reported by the ARCADE 2 collaboration, this is because they are dominated by noise and for this reason we just simply disregard them. Moreover, we have placed an upper limit $\Delta m_1 < 2.5 \times 10^{-4}\,\text{eV}$, corresponding to frequencies $\nu < 60\,\text{GHz}$, since at higher frequencies there are very stringent constraints from the FIRAS measurements [2]. Notice that an explanation of the excess radio background detected by ARCADE 2 in term of relic neutrino decays (or even in terms of any other relic particle decays), necessarily implies $E \leq \Delta m_1$ and, therefore, the *existence of an endpoint* $E_{\rm max} = \Delta m_1$. This is a very clear prediction of the model that will be tested by next experiments aiming at detecting deviations from CMB such as PIXIE, with low threshold $\nu_{\rm PIXIE} = 30\,\text{GHz}$ [18] and new radio interferometers such as TMS, with low threshold $\nu_{\rm TMS} = 10\,\text{GHz}$ [21, 22]. This implies that, for a fixed value of $\Delta m_1$, the model predicts no excess radiation at all energies $E > \Delta m_1$, so that the standard case is recovered. For this reason, in each interval $E_i < \Delta m_1 \leq E_{i+1}$ one has that the $\chi^2(\Delta m_1, \tau_1)$ varies continuously with $\Delta m_1$ but at each borderline energy value $E_i$ one has a discontinuity since the predicted temperature jumps from zero, for $\Delta m_1 \leq E_i$, to some finite value, for $\Delta m_1 > E_i$. Therefore, we determined the $\chi^2_{\rm min}$, and the best fit values, separately for each interval. Instead of $\tau_1$, we have minimised $\chi^2$ as a function of the quantity $A \equiv \Delta m_1^{3/2}\,\tau_1$ as a first parameter, together with $\Delta m_1$ as a second parameter. This is because, in the matter-dominated regime, $A$ is the only parameter that determines the effective temperature as one can see from eq. (3.2). In the left panel of figure 1 we show the $\chi^2$ per degrees of freedom (d.o.f.) as a function of $\Delta m_1^2$ for a fixed value of $A = \bar{A}_i$ in each interval $E_i \leq \Delta m_1 < E_{i+1}$, where $\bar{A}_i$ is the best fit value in that interval. One can clearly notice the jumps at each value $E_i$. For $\Delta m_1 < E_1$, one recovers the value $\chi^2_{\rm null} = 17.2$ (4 d.o.f.) corresponding to the standard case, since there is no observable quantity that can distinguish between the two cases. The results of the fit are shown in table 2 for each interval: we show best fit values for $A$, $\Delta m_1$ and $\tau_1$ and corresponding $\chi^2_{\rm min}$.

In the right panel of figure 1 we show the $\chi^2$ per d.o.f. as a function of $A$ for the best fit value of $\Delta m_1$ in each interval as indicated. For sufficiently large values of $A$ (i.e., large values of $\tau$), one again always recovers the standard case with $\chi^2_{\rm null} = 17.2$ (4 d.o.f.). In table 2 we



JCAP04(2024)046

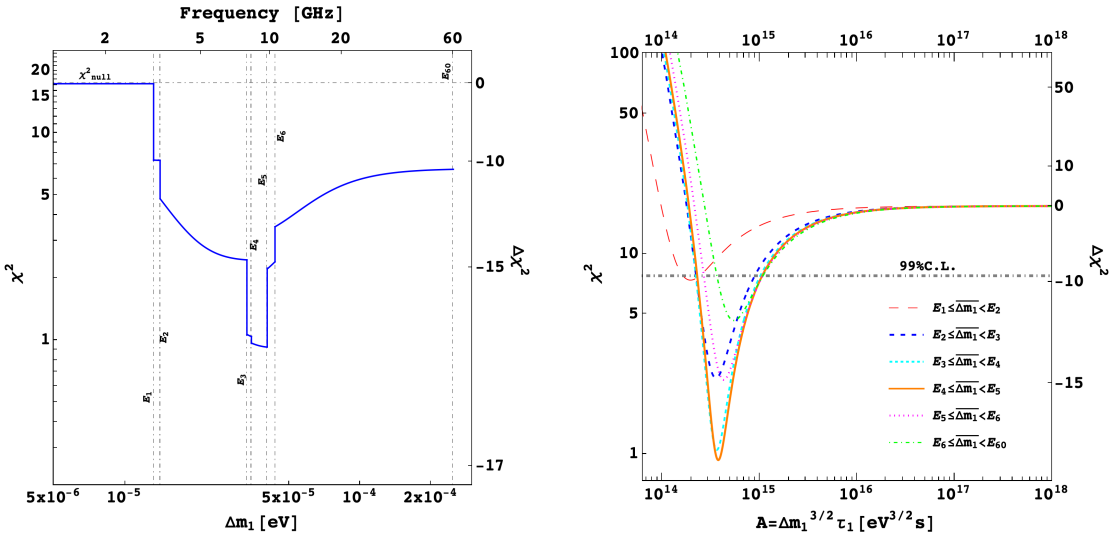


**Figure 1.** Left panel: $\chi^2$ versus $\Delta m_1$ for best fit value of $A$ in each interval as in table 2. Right panel: $\chi^2$ (4 d.o.f.) as a function of $A$ for the best fit values of $\Delta m_1$ in each interval $E_i \leq \Delta m_1 < E_{i+1}$ as in table 2.

| Interval | $\overline{A}$ (eV$^{3/2}$ s) | $\overline{\Delta m_1}$ (eV) | $\overline{\tau}_1$ (s) | $\chi^2_{\rm min}$ | $\Delta\chi^2_{\rm min}$ |
|---|---|---|---|---|---|
| $E_1 \leq \Delta m_1 < E_2$ | $1.9 \times 10^{14}$ | $1.4 \times 10^{-5}$ | $3.6 \times 10^{21}$ | 7.36 | $-9.87$ |
| $E_2 \leq \Delta m_1 < E_3$ | $2.3 \times 10^{14}$ | $2.7 \times 10^{-5}$ | $1.6 \times 10^{21}$ | 2.28 | $-14.95$ |
| $E_3 \leq \Delta m_1 < E_4$ | $3.6 \times 10^{14}$ | $3.4 \times 10^{-5}$ | $1.8 \times 10^{21}$ | 1.06 | $-16.17$ |
| $E_4 \leq \Delta m_1 < E_5$ | $3.8 \times 10^{14}$ | $4.0 \times 10^{-5}$ | $1.46 \times 10^{21}$ | 0.96 | $-16.27$ |
| $E_5 \leq \Delta m_1 < E_6$ | $4.2 \times 10^{14}$ | $4.3 \times 10^{-5}$ | $1.49 \times 10^{21}$ | 2.19 | $-15.04$ |
| $E_6 \leq \Delta m_1 < E_{60}$ | $4.7 \times 10^{14}$ | $2.0 \times 10^{-4}$ | $1.66 \times 10^{20}$ | 3.23 | $-14.00$ |

**Table 2.** Results of the fit of ARCADE 2 data. Best fit values, $\chi^2$ and $\Delta\chi^2$ are shown for each interval of $\Delta m_1$, corresponding to a frequency interval between two data points.

also show the different values $\Delta\chi^2_{{\rm min},i} = \chi^2_{{\rm min},i} - \chi^2_{\rm null}$. It is intriguing that the data points seem to indicate the presence of an end point falling in the interval $E_4 < E \sim 4\times10^{-5}\,{\rm eV} \leq E_5$ ($\nu_4 < \nu \simeq 9.7\,{\rm GHz} < \nu_5$) as also confirmed by the results of the fit: the best fit is found indeed for $E_4 < \Delta m_1 \lesssim E_5 = 4.02 \times 10^{-5}\,{\rm eV}$ with $\chi^2_{{\rm min},4} = 0.96$. In figure 2 we show the best fit curves for $T_{\gamma_{\rm nth}}(E, 0)$ for each interval together with the six ARCADE 2 data points. The thick solid (orange) curve corresponds to the global best fit and it should be clear how well it fits all data points. In figure 3 we show the resulting 99% C.L. allowed region in the plane of $\Delta m_1$ versus $\tau_1$. The different blue shades are indicative of the goodness of the fit. The orange star denotes the global best fit.

If we focus on the interval $E_4 \leq \Delta m_1 < E_5$, where the best fit is found, we find $\overline{A} \simeq 3.8\times10^{14}\,{\rm eV}^{3/2}\,{\rm s}$ with $\chi^2_{\rm min}/{\rm d.o.f.} \simeq 0.96$ (4 d.of.). For $\chi^2 \lesssim \chi^2_{\rm min} + (2.6)^2$, (corresponding approximately to the 99% C.L. range), we find

$$A = 3.8^{+7.2}_{-1.5} \times 10^{14}\,{\rm eV}^{3/2}\,{\rm s}\,. \tag{3.3}$$



JCAP04(2024)046

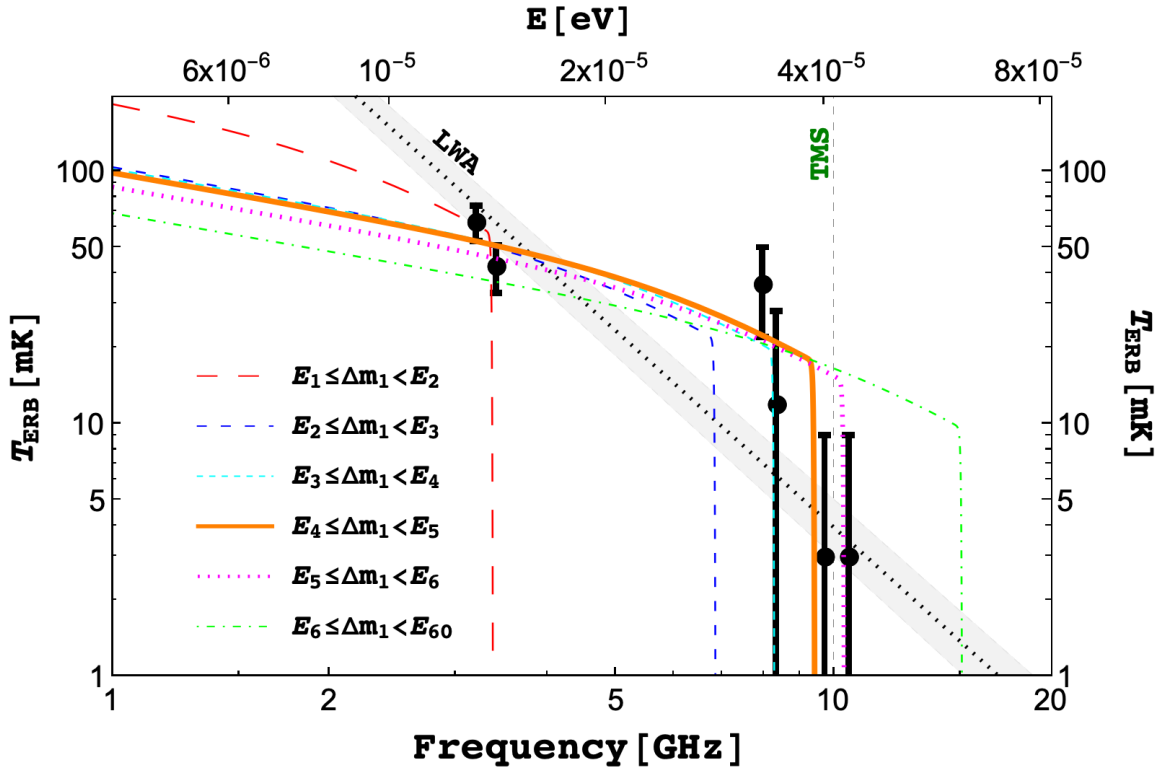


**Figure 2.** Best fit curves for $T_{\rm ERB}$ obtained with eq. (3.2). The thick solid orange curve corresponds to a solution very close to the best global fit ($\Delta m_1 = 4.0 \times 10^{-5}\,\text{eV}$ and $\tau_1 = 1.46 \times 10^{21}\,\text{s}$). The ARCADE 2 data points are taken from ref. [1], while the power-law fit $\beta = -2.58 \pm 0.05$ (dotted line with grey shade) is from [3].

If one interprets the ARCADE 2 excess as due to some alternative explanation than relic neutrino decays, then (3.3) places the 99% C.L. lower bound

$$(\Delta m_1)^{3/2}\,\tau_1 > 2.3(1.3) \times 10^{14}\,\text{eV}^{3/2}\,\text{s}\,, \tag{3.4}$$

that, as one can see from figure 3, approximately holds in the range $2.5 \times 10^{-5}\,\text{eV} < \Delta m_1 < E_{60} = 2.5 \times 10^{-4}\,\text{eV}$ ($E_1 = 1.36 \times 10^{-5}\,\text{eV} \leq \Delta m_1 \leq 2.5 \times 10^{-5}\,\text{eV}$). The ARCADE 2 data can be combined with additional data also providing evidence for an excess radio background at lower frequencies ($40\,\text{MHz} \lesssim \nu \lesssim 1.42\,\text{GHz}$) and in this case a power law yields a very good combined fit [1]. More recently, the Long Wavelength Array (LWA) measured the diffuse radio background between 40 and 80 MHz, also finding an excess. In combination with the data from ARCADE 2 and other experiments, the following power law spectrum has been found [3]

$$T_{\rm ERB} = (30.4 \pm 2.6)\left(\frac{\nu}{310\,\text{MHz}}\right)^{-2.58\pm0.05}\,\text{K}\,. \tag{3.5}$$

This is shown in figure 2 with a grey band. It can be seen however that especially the third point from ARCADE 2 seems not to be well fit by this power law. One indeed finds $\chi^2 \simeq 2.5$ (4 d.o.f.), showing that the power law in eq. (3.5) gives a worse fit to the ARCADE 2 data than the best fit we found, but it is still acceptable. However, the power law in eq. (3.5) still



JCAP04(2024)046

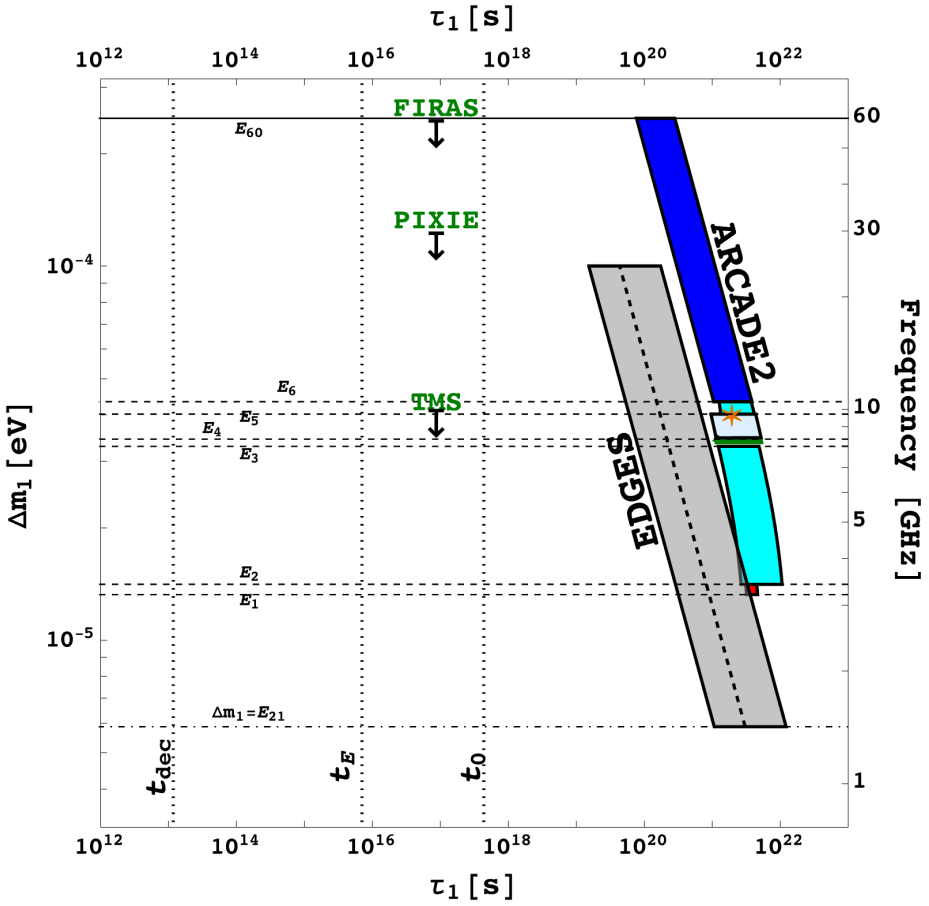


**Figure 3.** Allowed region in the plane of $\Delta m_1$ versus $\tau_1$ (99% C.L.). The orange star indicates the best fit to ARCADE 2 excess found. Colour code: light grey for $\chi^2 < 1$, green for $1 < \chi^2 < 2$, cyan for $2 < \chi^2 < 3$, blue for $3 < \chi^2 < 7$ and red for $7 < \chi^2 < 9$. We also show the best-fit and 99% C.L. region for the EDGES anomaly (dashed line and grey shaded region). The vertical lines show (from left to right) the epochs of CMB decoupling, cosmic dawn and the age of the Universe. The horizontal lines correspond to different photon energies (or frequencies). The region above 60 GHz is disfavored by FIRAS, and this limit can be improved down to 30 GHz with PIXIE, or to 10 GHz by TMS, as shown by the downward arrows.

requires some physical source that produces it. It is then legitimate to wonder whether it is possible to combine the success of relic neutrino decays in reproducing the ARCADE 2 data with the success of the power law (3.5) in reproducing data below 1 GHz. As recently pointed out in [25], the account of soft photon heating from free-free processes might provide a plausible solution to find such a combined description of ARCADE 2 with sub-GHz data. In this case the power law would hold up to $\nu \sim 1\,\mathrm{GHz}$ but should turn into eq. (3.2) at higher frequencies. Testing such a hypothesis of course would require a new experiment able to collect data points in the 1 GHz–20 GHz range. The TMS experiment will only take data above 10 GHz. This will be certainly still useful to strengthen the hint for the existence of an endpoint and possibly rule out the validity of the power law in eq. (3.5) up to such high frequencies. However, it will not provide a thorough test of the best fit solution we found to



JCAP04(2024)046

the excess radio background. This could come from a new balloon experiment, an improved version of ARCADE 2. Of course an accurate and precise agreement with the prediction from eq. (3.2) could provide a strong evidence (if not a 'smoking gun').

## 4 Predicting the 21 cm cosmological global absorption signal

An additional 'smoking gun test' of our relic neutrino decay hypothesis, which predicts non-thermal photons also at higher redshifts, can be provided by the observation of the 21 cm cosmological global absorption signal. The 21 cm hyperfine transition of the hydrogen atom can be used to test the physics of the cosmic dawn, when first astrophysical sources start to form [53]. It is a transition between the spin-singlet and triplet levels of the 1s ground state of the hydrogen atom. The energy gap at rest, giving the energy of the absorbed or emitted photons in the transition, is $E_{21} = 5.87\,\mu\text{eV}$ corresponding to a 21 cm line rest frequency $\nu_{21}^{\rm rest} = 1420\,\text{MHz}$. The ratio of the population of the excited (spin-triplet) state, $n_1$, to that one of the ground (spin-singlet) state, $n_0$, can be parameterised in terms of a *spin temperature* $T_{\rm S}(z)$ depending on the redshift:

$$\frac{n_1}{n_0}(z) \equiv \frac{g_1}{g_0}\, e^{-\frac{E_{21}}{T_{\rm S}(z)}}\,, \tag{4.1}$$

where $g_1/g_0 = 3$ is the excited state-to-ground state degeneracy ratio. The possibility to detect an observable signal from the 21 cm cosmological transitions of the hydrogen atoms in the primordial gas after recombination relies on a non-vanishing *brightness constrast* between the cosmic radiation and the radiation emitted in the 21 cm transitions. This can be parameterised in terms of the 21cm brightness temperature $T_{21}(z)$ [54]

$$T_{21}(z) \simeq 23\,\text{mK}\,(1+\delta_{\rm B})\,x_{H_I}(z)\left(\frac{\Omega_{\rm B0}h^2}{0.02}\right)\left[\left(\frac{0.15}{\Omega_{\rm M0}h^2}\right)\left(\frac{1+z}{10}\right)\right]^{1/2}\left[1-\frac{T_\gamma(z)}{T_{\rm S}(z)}\right], \tag{4.2}$$

where $\delta_{\rm B} = (\rho_{\rm B} - \bar{\rho}_{\rm B})/\bar{\rho}_{\rm B}$ is the fractional baryon overdensity, $x_{H_I}(z)$ is the neutral hydrogen fraction, $\Omega_{\rm B0}$ and $\Omega_{\rm M0}$ are the baryon and matter energy density parameters, $h$ is the Hubble constant in units of $100\,\text{km}\,\text{s}^{-1}\,\text{Mpc}^{-1}$. If the spin temperature is equal to the photon temperature ($T_{\rm S} = T_\gamma$), then photons are absorbed and reemitted with the same intensity and there is no visible signal. Also, if all atoms are ionised so that $x_{H_I} = 0$, there cannot be any signal. Another important point to consider is that the spin temperature is related to $T_{\rm gas}$, the kinetic temperature of the gas, by

$$\left(1-\frac{T_\gamma}{T_{\rm S}}\right) \simeq \frac{x_c + x_\alpha}{1 + x_c + x_\alpha}\left(1-\frac{T_\gamma}{T_{\rm gas}}\right), \tag{4.3}$$

where $x_\alpha$ and $x_c$ are coefficients describing the coupling between the hyperfine levels and the gas. Specifically, the $x_c$ term is for collisional excitation of the hyperfine transition, and the $x_\alpha$ term is for the Wouthuysen-Field effect, mediated by the absorption and subsequent re-emission of a Lyman-$\alpha$ photon. In the limit of strong coupling, for $x_\alpha + x_c \gg 1$, one has $T_{\rm S} = T_{\rm gas}$, while in the limit of no coupling, for $x_\alpha = x_c = 0$, one has $T_{\rm S} = T_\gamma$ and in this case also there is no signal.



JCAP04(2024)046

From these considerations, one can then draw the following evolution for the 21cm global signal [24, 53]:

(i) The hydrogen gas decouples completely from the cosmic radiation, so that one can have $T_{\rm S} \neq T_\gamma$, at a redshift $z_{\rm dec} \simeq 150$. For lower redshifts, the gas cools down more rapidly than cosmic radiation, with $T_{\rm gas}(z) = T(z_{\rm dec})\,(1+z_{\rm dec})^2$. Moreover in the redshift range $z_{\rm dec} \gtrsim z \gtrsim 30$, the gas collision rate is high enough that the 21 cm transitions are coupled to the gas temperature and approximately $T_{\rm S} \simeq T_{\rm gas}$. During this stage an absorption signal, for $T_{21} < 0$, is expected.

(ii) At redshifts $z \simeq 30$, the gas becomes so rarified that collisions are unable to couple the spin temperature to the gas temperature and one has $x_a + x_c \ll 1$ and $T_{\rm S} \simeq T_\gamma$. Therefore, at this stage $T_{21} \simeq 0$ and there is no 21 cm signal again.

(iii) At redshifts $z_\star \simeq 30$, first luminous sources also start to form and this, via Wouthuysen-Field effect, triggers a gradual re-coupling of the 21 cm transitions with the gas so that the spin temperature gradually tends again to the gas temperature. In this stage one can again expect an absorption signal since $T_{21} < 0$.

(iv) Finally, for redshifts around $z \simeq 10$, the gas gets reheated by the astrophysical radiation and the gas temperature increases. In this stage it might even be possible to have $T_{\rm S} \simeq T_{\rm gas} > T_\gamma$, so that one has an emission signal from regions where the gas is not fully ionised. All gas gets eventually ionised, so that the signal switches off again.

The EDGES collaboration has found an absorption profile in the range $z = 15$–$20$, with the minimum at a frequency $\nu_{21}(z_E) \simeq 78\,{\rm MHz}$ corresponding to $z_E \simeq 17$ [26]. The absorption profile has a U shape with quite a flat minimum. We do not attempt at fitting the precise shape of the profile since this may be sensitive to systematic errors and the assumed form of the fitted model. However, we will take into account that the exact frequency of the minimum and, consequently, its redshift has an uncertainty and one can actually write $z_E = \bar{z}_E \pm 1$. Let us first focus on the central value $\bar{z}_E = 17$. At this value, the ΛCDM model predicts a relic photon temperature

$$T_\gamma(\bar{z}_E) = T(\bar{z}_E) = T_0\,(1+\bar{z}_E) \simeq 49.6\,{\rm K}\,, \tag{4.4}$$

and a gas temperature $T_{\rm gas}(\bar{z}_E) \simeq 7.2\,{\rm K}$.[5] Defining $\xi(z) \equiv T_\gamma(z)/T_{\rm gas}(z)$, one has then $\xi(\bar{z}_E) \simeq 6.89$, corresponding, to $T_{21}(\bar{z}_E) \simeq -206\,{\rm mK}$ from eq. (4.2).[6]

On the other hand, the EDGES collaboration finds a much stronger absorption signal with $T_{21}^{\rm EDGES}(z_E) = -500^{+200}_{-500}\,{\rm mK}$ (99% C.L.). From eq. (4.2), this translates into

$$\xi^{\rm EDGES}(\bar{z}_E) = 15.1^{+14.1}_{-5.6}\,, \tag{4.5}$$

[5] Assuming an instantaneous decoupling, one can approximately estimate the gas temperature as

$$T_{\rm gas}(\bar{z}_E) \simeq T(z_{\rm dec})\,\frac{(1+\bar{z}_E)^2}{(1+z_{\rm dec})^2} \simeq 6\,{\rm K}\,.$$

The more accurate result in the text comes from a solution of kinetic equations [55].

[6] We are using $\Omega_{\rm M0}h^2 = 0.1424$ and $\Omega_{\rm B0}h^2 = 0.02242$ [50].



JCAP04(2024)046

and from this one finds first

$$T_{\gamma}^{\rm EDGES}(\bar{z}_E) = \xi^{\rm EDGES}(\bar{z}_E)\, T_{\rm gas}(\bar{z}_E) = 109^{+101}_{-41}\,{\rm K}\,, \tag{4.6}$$

and then finally, subtracting the temperature of thermal photons, one obtains for the effective temperature of the non-thermal contribution (99% C.L.)

$$T_{\gamma_{\rm nth}}^{\rm EDGES}(\bar{z}_E) = (60^{+101}_{-41})\,{\rm K}\,. \tag{4.7}$$

Finally, we have also calculated the additional error coming from the uncertainty $\Delta z_E = \pm 1$ and found that this is of order of 3 K so that, once added in quadrature, it gives a negligible increase of 0.1 K to the total error.

Eq. (4.7) is the experimental quantity we need to reproduce. We have now to use eq. (2.8) to calculate the effective temperature from the specific intensity and eq. (2.1) for the specific intensity of photons produced from relic neutrino decays. This time, in the case of EDGES, the redshift is $z_E$ and the energy is $E_{21}$, so that we obtain

$$T_{\gamma_{\rm nth}}(E_{21}, z_E) \simeq \frac{6\,\zeta(3)}{11\,\sqrt{\Omega_{\rm M0}}}\,\frac{T_0^3\,(1+z_E)^{3/2}}{E_{21}^{1/2}\,\Delta m_1^{3/2}}\,\frac{t_0}{\tau_1}\,, \tag{4.8}$$

where we have again neglected the exponential, considering the case $\tau_1 \gg t(z_E)$, and we used the approximation $H(a_{\rm D}) \simeq H_0\,\sqrt{\Omega_{M0}}\,(1+z_E)^{3/2}\,(\Delta m_1/E_{21})^{\frac{3}{2}}$, holding in the matter-dominated regime. Imposing that this predicted effective temperature reproduces the experimental measurement in eq. (4.7), one finds (99% C.L.)

$$A^{\rm EDGES}(\bar{z}_E) = \frac{6\,\zeta(3)}{11\,\sqrt{\Omega_{\rm M0}}}\,\frac{T_0^3\,(1+\bar{z}_E)^{3/2}}{T_{\gamma_{\rm nth}}^{\rm EDGES}(\bar{z}_E)\,E_{21}^{1/2}}\,t_0 = (4.0^{+8.8}_{-2.5})\times 10^{13}\,{\rm eV}^{3/2}\,{\rm s}. \tag{4.9}$$

This result holds in the range $E_{21} = 5.87\,\mu{\rm eV} \leq \Delta m_1 \lesssim 10^{-4}\,{\rm eV}$. The lower bound is clear since only photons produced with energies above $E_{21}$ at redshifts $z_{\rm D} \geq z_E$ can excite the Hydrogen atom ground states. The upper bound is due to the fact that we are treating neutrinos as non-relativistic at decay. Therefore, one has to impose $T_\nu(z_{\rm D}) \lesssim m_1/3 \lesssim 0.05\,{\rm eV}$, where in the last inequality we have used the upper bound $m_1 \lesssim 0.015\,{\rm eV}$ coming from *Planck* data [50].[7] This implies $1+z_{\rm D} \lesssim 300$ and consequently $\Delta m_1 \lesssim E_{21}(1+z_{\rm D})/(1+z_E) \sim 10^{-4}\,{\rm eV}$.

The resulting (99% C.L.) allowed region in the plane of $\Delta m_1$ versus $\tau_1$ is shown in figure 3 in light grey. This has to be compared with the allowed region obtained fitting ARCADE 2 data in eq. (3.3). It is clear that the two regions only marginally overlap and so there is some tension between the two results. This tension might be reconciled if the current EDGES measurement is overestimating the 21 cm global absorption signal.

[7] We are using a conservative upper bound on the sum of the neutrino masses (95% C.L.) [50]

$$\sum_i m_i < 0.44\,{\rm eV}\,,$$

derived just from *Planck* data (no BAO), combining temperature anisotropies (TT), low E polarisation data and lensing. The use of such conservative bound is justified by the existing cosmological tensions, that support cosmological models beyond the minimal ΛCDM model resulting in a relaxation of the upper bound on neutrino masses.



JCAP04(2024)046

Reversely, it is easy to derive a prediction for the contrast brightness temperature $T_{21}$, that future 21 cm cosmology experiments should measure, starting from our ARCADE 2 data fit. This can be simply done plugging first eq. (3.3), giving the (99% C.L.) allowed range for $A$ from ARCADE 2 data at the best fit value for $\Delta m_1$, into eq. (4.8), finding $T_{\gamma_{\rm nth}}(E_{21}, z_E)$, and then from eq. (4.2) one obtains (99% C.L.):

$$T_{21}(\bar{z}_E) = -238^{+21}_{-20}\,\mathrm{mK}\,. \tag{4.10}$$

When this is compared with the EDGES measurement, unsurprisingly, one again finds the same kind of tension found in terms of $A$, now expressed in terms of the observable $T_{21}$. The result (4.10) is one of our main results, since it is another clear prediction of the model. This, together with a test of the predictions of the excess radio background effective temperature, represents a clear signature of the model.

## 5 On dark matter decays/de-excitations as alternative explanation

The solution we have found can also be mimicked by replacing relic neutrino decays with dark matter decays or de-excitations. This kind of models was proposed as explanation the EDGES anomaly [44].[8] For example, one can have in mind a picture where dark matter is made of some dark atoms and photons are produced from de-excitations of the first excited state into the ground state. Indicating with $m_{\rm DM}$ the mass of dark matter and with $f_{\rm D}$ the fraction of dark matter abundance in the excited state, we obtain for the effective temperature of the excess radio background

$$T^{(\rm DM)}_{\gamma_{\rm nth}}(E,0) = \frac{\pi^2\, f_{\rm D}\, n^{\infty}_{\rm DM}(0)}{E^2}\, \frac{e^{-\frac{t(a_{\rm D})}{\tau_{\rm DM}}}}{H(a_{\rm D})\,\tau_{\rm DM}}\,. \tag{5.1}$$

The (average) dark matter number density at the present time is simply given by

$$n^{\infty}_{\rm DM}(0) = \frac{\rho_{\rm c0} h^{-2}}{m_{\rm DM}}\,\Omega_{\rm DM0}h^2 \simeq 1.26\,\frac{\rm GeV}{m_{\rm DM}}\,\mathrm{m}^{-3}\,, \tag{5.2}$$

where we used $\Omega_{\rm DM0}h^2 = 0.11933$ [50] and $\rho_{\rm c0}h^{-2} = 10.54\,\mathrm{GeV\,m^{-3}}$, with $\rho_{\rm c0}$ the critical energy density at the present time. In terms of the neutrino number density $n^{\infty}_{\nu_1}(0)$ (see eq. (2.2)), it can also be rewritten as

$$n^{\infty}_{\rm DM}(0) = \frac{11.3\,\mathrm{eV}}{m_{\rm DM}}\, n^{\infty}_{\nu_1}(0)\,. \tag{5.3}$$

In this way the effective temperature of the excess radio background from dark matter de-excitations can be expressed in terms of the one we found for relic neutrino decays (eq. (3.2)):

$$T^{(\rm DM)}_{\gamma_{\rm nth}}(E,0) = \left(\frac{11.3\,\mathrm{eV}}{m_{\rm DM}\, f_{\rm D}^{-1}}\right)\, \frac{\tau_1}{\tau_{\rm DM}}\, T^{(\nu)}_{\gamma_{\rm nth}}(E,0)\, e^{-\frac{t(a_{\rm D})}{\tau_{\rm DM}}}\,. \tag{5.4}$$

[8] In this case, one should use eq. (2.1) with $n^{\infty}_{\nu_1}(z_E)$ replaced by $n^{\infty}_{\rm DM}(z_E)$, the number density of excited dark matter at the redshift $z_E$. However, in [44] the number density of excited dark matter at the present time, $n^{\infty}_{\rm DM,0}$, was used, as in the case of ARCADE 2 excess radio background, that is a factor $(1+z_E)^3$ smaller.



JCAP04(2024)046

| $m_{\rm DM}/f_{\rm D}$ | $\chi^2_{\rm min}$ | $\bar{\tau}_{\rm DM}$ |
|---|---|---|
| 11.3 eV | 0.96 | $1.46 \times 10^{21}$ s |
| 100 eV | 0.97 | $1.67 \times 10^{20}$ s |
| 1 keV | 0.98 | $1.67 \times 10^{19}$ s |
| 10 keV | 1.15 | $1.68 \times 10^{18}$ s |
| 100 keV | 6.6 | $1.4 \times 10^{17}$ s |

**Table 3.** Values of $\chi^2_{\rm min}$ and $\bar{\tau}_{\rm DM}$ for some increasing values of $m_{\rm DM}/f_{\rm D}$.

If we approximate $t(a_{\rm D}) \simeq t_0$, strictly valid for $E = \Delta m_1$, then it is clear that the same solution we obtained for neutrinos is also obtained for dark matter decays/de-excitations replacing $\tau_1 \to \tau_{\rm DM}$ (and of course $\Delta m_1 \to \Delta m_{\rm DM}$) for

$$m_{\rm DM}\, f_{\rm D}^{-1} \sim 10\,{\rm keV} \frac{t_0}{\tau_{\rm DM}}\, e^{-\frac{t_0}{\tau_{\rm DM}}}\,. \tag{5.5}$$

As long as $\tau_{\rm DM} \gtrsim t_0$, the exponential does not play any role. One can see that for $m_{\rm DM}/f_{\rm D} \sim 10\,{\rm eV}$, one obtains the same value of the lifetime we obtained for neutrinos, $\tau_{\rm DM} \sim \bar{\tau}_1 \sim 10^{21}\,{\rm s}$. For increasing values of $m_{\rm DM}/f_{\rm D}$, the lifetime, and therefore the value of $A$, decreases as $\tau_{\rm DM} \propto (m_{\rm DM}/f_{\rm D})^{-1}$. For $m_{\rm DM}/f_{\rm D} \sim 10\,{\rm keV}$, one has $\tau_{\rm DM} \sim t_0$. In this case, the exponential kicks in and the effective temperature starts to be suppressed exponentially. This occurs because the dark matter number density, and correspondingly the specific intensity, starts to become too low. Therefore, the ARCADE 2 data cannot be reproduced for values of $m_{\rm DM}/f_{\rm D}$ much larger than 10 keV and one obtains the approximate upper bound

$$m_{\rm DM} \lesssim 10\,{\rm keV}\, f_{\rm D}\,. \tag{5.6}$$

Notice though that one can still reproduce the EDGES data since in that case one has to replace $t_0 \to t_E = t(\bar{z}_E) \simeq 250\,{\rm Myr} \sim 10^{16}\,{\rm s}$. In this case the upper bound relaxes by about two orders of magnitude. Of course in this case it would be impossible to reconcile EDGES anomaly and ARCADE 2 excess radio background. We have also derived this upper bound numerically, using eq. (5.4) to fit the ARCADE 2 data, calculating the $\chi^2$, as we did in the case of neutrino decays, for a few values of $m_{\rm DM}/f_{\rm D}$. In this case, however, the exponential has to be taken into account, since it plays a crucial role in placing the upper bound. Fixing $\Delta m_{\rm DM} = 4 \times 10^{-5}\,{\rm eV}$, the best fit value obtained for $\Delta m_1$ in the case of relic neutrino decays, we show in table 3 the values of $\chi^2_{\rm min}$ (4 d.o.f.) and $\bar{\tau}_{\rm DM}$ we have obtained for some (increasing) values of $m_{\rm DM}/f_{\rm D}$.

As one can see, for $m_{\rm DM}/f_{\rm D} = 11.3\,{\rm eV}$, one recovers the same best fit obtained for relic neutrino decays. For $m_{\rm DM}/f_{\rm D} \gtrsim 10\,{\rm keV}$, the fit rapidly deteriorates and one obtains an upper bound $m_{\rm DM}/f_{\rm D} \lesssim 100\,{\rm keV}$ at about 99% C.L.. For larger values, one recovers the null hypothesis, since the dark matter number density becomes so low that the predicted values of the effective temperature become much lower than the measured ones for any value of $\tau_{\rm DM}$. Notice that, compared to the simple analytical estimate eq. (5.6), the upper bound is somehow relaxed. This is because the values $t(a_{{\rm D},i})$, obtained for $a_{{\rm D},i} = E_i/\Delta m_{\rm DM}$, are one-two orders of magnitude smaller than $t_0$.



JCAP04(2024)046

We should also make clear that this upper bound on the dark matter mass is obtained under the assumptions of validity of the solution. In particular, this holds under the assumption that the excess radio background is explained by the primary photons produced from dark matter decays/de-excitations that are simply redshifted from decays to the present time in case of the excess radio background or to $t_E$ in the case of the EDGES anomaly. This does not exclude that other processes, such as soft photon heating, could be active at higher dark matter mass or mass difference values, reprocessing injected photons and reproducing the excess radio background, though with a different spectrum, typically a power law one [25].

Finally, notice that these strong limitations on a solution in terms of dark matter decays/de-excitations are in addition to the strong constraints from the smoothness of the excess radio background that clashes with the expected anisotropies of the signal that should track the dark matter density distribution.[9]

## 6 Final remarks

Let us conclude with some final remarks on the solution to the excess radio background we have discussed.

- We have referred to the case of lightest neutrino decays into sterile neutrinos. However, as we said in the introduction, the discussion is equally applicable to the case when one of the two heavier light neutrinos, either $\nu_2$ or $\nu_3$, decays into sterile neutrinos; simply one has to replace everywhere $\Delta m_1 \to \Delta m_{2,3}$ and $\tau_1 \to \tau_{2,3}$. The difference is that $m_2$ and $m_3$ are lower-bounded by the solar neutrino and atmospheric neutrino mass scales, respectively, i.e., $m_2 \gtrsim 8\,\text{meV}$ and $m_3 \gtrsim 50\,\text{meV}$ (in this case $m_1$ can be arbitrarily small). This lower bound guarantees they are automatically non-relativistic in all the relevant range of redshifts (0–300). On the other hand, in the case of lightest active neutrinos, we have to impose $m_1 \gtrsim 10\,\text{meV}$, an interesting condition that might be tested during next years by absolute neutrino mass scale experiments (including cosmology). It is also intriguing to notice that since the clustering of neutrinos is proportional to their mass, then in principle excess radio background anisotropies, either a detection or also an upper bound, would allow to distinguish among the three cases and even give information on the absolute neutrino mass scale.

- The solution we found predicts an effective temperature of the excess radio background that depends on photon energy as $\propto E^{-0.5}$ for $a_\text{D} = E/\Delta m_i \lesssim a_\text{eq} \simeq 0.75$ and as $\propto E^{-1.5}$ for $a_\text{D} \gtrsim 0.75$, with an abrupt endpoint at $E = \Delta m_i$. These are all features that makes it distinguishable from other solutions and in particular from the power law eq. (3.5). To this extent measurements in the frequency range $\nu = 1$–$20\,\text{GHz}$ would be needed and so an improved ARCADE 2-like experiment would be certainly a priority. The TMS microwave telescope, will only partly test the solution at $\nu \geq 10\,\text{GHz}$. The

[9] In [8], a 95% C.L. upper bound of 1% has been derived on the clustering amplitude at small scales (between 300 kpc and 3 Mpc) using ATCA data at 8.7 GHz [56]. On the other hand, expected clustering amplitude from radio sources tracking matter distribution, as it would be of course the case of decaying dark matter, is about 5 times higher. This clearly rules out these models, at least in their minimal version. One has to introduce some *ad hoc* smoothing mechanism to rescue them.



JCAP04(2024)046

best fit solution we found predicts that no excess will be detected at TMS. On the other hand, one expects that the power law, well describing the excess radio background measurements at low frequencies, should be recovered accounting for processes such as soft photon heating reprocessing lower frequency photons.

- As pointed out in [15], there is a second solution for life-times much shorter than the age of the universe. In this case the exponential in eq. (3.2) cannot be neglected. However, this solution is strongly fine-tuned and it lives only within a very narrow range of $A$ values. In addition, for such short life-times, free-free processes should be taken into account. Moreover, this solution predicts a negligible deviation in the absorption 21 cm cosmological signal from the standard case, so that the tension with the EDGES anomaly is even more exacerbated.

- The excess radio background is a detection of photons produced by relic neutrino decays at relatively low redshifts (the highest redshift for the best fit solution is given by $z \simeq E_5/E_1 - 1 \simeq 2$). However, the 21 cm global signal is also sensitive to photons produced at higher redshifts (up to $\sim 300$). In particular, we have seen how the solution for the excess radio background predicts $T_{21} \simeq -240\,\mathrm{mK}$. This is another very specific prediction that will be tested during next years. This prediction is in mild tension with the anomalous EDGES measurement of the 21 cm absorption global signal. A possible explanation is that this might have been overestimated due to some unidentified foreground.

- The same solution we found in the case of relic neutrino decays could also be mimicked by decays/de-excitations of some fraction $f_{\rm D}$ of (cold/warm) dark matter. However, this solution is only possible for masses $m_{\rm DM}/f_{\rm D} \lesssim 10\,\mathrm{keV}$. This limitation is in addition to the difficulty of such solutions to explain the smoothness of the excess radio background, since they unavoidably predict anisotropies tracking the dark matter density distribution.

- The solution we have presented assumes that the effect of stimulated decay, as considered in [57], is absent. This can be nicely realised within a model where neutrinos are unstable, and will be presented in a forthcoming paper [58].

- Our solution relies on the fact that there is a small mass splitting between the active and sterile neutrino components, or in other words, neutrinos are pseudo-Dirac (albeit with non-maximal mixing).[10] The cosmological probes proposed here are complementary to other laboratory [64–67] and astrophysical [60, 68–75] probes of pseudo-Dirac neutrinos.

It is quite exciting that radio background experiments have the opportunity during next years to test the stability of the cosmic neutrino background. The relic neutrino decay solution of the excess radio background we have discussed clearly relies on new physics and, therefore, it might provide a very important guidance toward an extension of our current established

[10] For concrete ultraviolet-complete model realizations of the pseudo-Dirac hypothesis, see e.g. [59, 60]. It is interesting to note that certain string landscape (swampland) constructions predict that neutrinos are necessarily pseudo-Dirac [61–63].



JCAP04(2024)046

fundamental theories of nature. In particular, it might help resolve the nature of neutrino mass — one of the fundamental open questions.

## Acknowledgments

The work of BD was partly supported by the U.S. Department of Energy under grant No. DE- SC 0017987. PDB and RR acknowledge financial support from the STFC Consolidated Grant ST/T000775/1. IMS is supported by STFC grant ST/T001011/1. This project has received funding from the European Union's Horizon Europe research and innovation programme under the Marie Skłodowska-Curie Staff Exchange grant agreement No. 101086085 – ASYMMETRY. In particular, PDB wishes to thank the MIT Center for Theoretical Physics for the hospitality and Tracy Slatyer for useful discussions. We also wish to thank Jens Chluba for useful comments.

## References

[1] D.J. Fixsen et al., *ARCADE 2 Measurement of the Extra-Galactic Sky Temperature at 3–90 GHz*, *Astrophys. J.* **734** (2011) 5 [arXiv:0901.0555] [INSPIRE].

[2] D.J. Fixsen and J.C. Mather, *The Spectral Results of the Far-Infrared Absolute Spectrophotometer Instrument on COBE*, *Astrophys. J.* **581** (2002) 817.

[3] J. Dowell and G.B. Taylor, *The Radio Background Below 100 MHz*, *Astrophys. J. Lett.* **858** (2018) L9 [arXiv:1804.08581] [INSPIRE].

[4] J. Singal et al., *The Radio Synchrotron Background: Conference Summary and Report*, *Publ. Astron. Soc. Pac.* **130** (2018) 036001 [arXiv:1711.09979] [INSPIRE].

[5] N. Fornengo, R.A. Lineros, M. Regis and M. Taoso, *The isotropic radio background revisited*, *JCAP* **04** (2014) 008 [arXiv:1402.2218] [INSPIRE].

[6] E. Todarello et al., *Constraints on the origin of the radio synchrotron background via angular correlations*, arXiv:2311.17641 [INSPIRE].

[7] T. Vernstrom, R.P. Norris, D. Scott and J.V. Wall, *The Deep Diffuse Extragalactic Radio Sky at 1.75 GHz*, *Mon. Not. Roy. Astron. Soc.* **447** (2015) 2243 [arXiv:1408.4160] [INSPIRE].

[8] G.P. Holder, *The unusual smoothness of the extragalactic unresolved radio background*, *Astrophys. J.* **780** (2014) 112 [arXiv:1207.0856] [INSPIRE].

[9] N. Fornengo, R. Lineros, M. Regis and M. Taoso, *Possibility of a Dark Matter Interpretation for the Excess in Isotropic Radio Emission Reported by ARCADE*, *Phys. Rev. Lett.* **107** (2011) 271302 [arXiv:1108.0569] [INSPIRE].

[10] J.M. Cline and A.C. Vincent, *Cosmological origin of anomalous radio background*, *JCAP* **02** (2013) 011 [arXiv:1210.2717] [INSPIRE].

[11] A. Caputo et al., *Radio excess from stimulated dark matter decay*, *Phys. Rev. D* **107** (2023) 123033 [arXiv:2206.07713] [INSPIRE].

[12] R. Brandenberger, B. Cyr and R. Shi, *Constraints on Superconducting Cosmic Strings from the Global* 21*-cm Signal before Reionization*, *JCAP* **09** (2019) 009 [arXiv:1902.08282] [INSPIRE].

[13] B. Cyr, J. Chluba and S.K. Acharya, *A cosmic string solution to the radio synchrotron background*, arXiv:2308.03512 [INSPIRE].



JCAP04(2024)046

[14] S. Mittal and G. Kulkarni, *Background of radio photons from primordial black holes*, *Mon. Not. Roy. Astron. Soc.* **510** (2022) 4992 [arXiv:2110.11975] [INSPIRE].

[15] M. Chianese, P. Di Bari, K. Farrag and R. Samanta, *Probing relic neutrino radiative decays with 21 cm cosmology*, *Phys. Lett. B* **790** (2019) 64 [arXiv:1805.11717] [INSPIRE].

[16] S.K. Acharya, J. Dhandha and J. Chluba, *Can accreting primordial black holes explain the excess radio background?*, *Mon. Not. Roy. Astron. Soc.* **517** (2022) 2454 [arXiv:2208.03816] [INSPIRE].

[17] S.K. Acharya and J. Chluba, *A closer look at dark photon explanations of the excess radio background*, *Mon. Not. Roy. Astron. Soc.* **521** (2023) 3939 [arXiv:2209.09063] [INSPIRE].

[18] A. Kogut et al., *The Primordial Inflation Explorer (PIXIE): A Nulling Polarimeter for Cosmic Microwave Background Observations*, *JCAP* **07** (2011) 025 [arXiv:1105.2044] [INSPIRE].

[19] A. Kogut et al., *CMB Spectral Distortions: Status and Prospects*, *Bull. Am. Astron. Soc.* **51** (2019) 113 [arXiv:1907.13195] [INSPIRE].

[20] J. Chluba et al., *New horizons in cosmology with spectral distortions of the cosmic microwave background*, *Exper. Astron.* **51** (2021) 1515 [arXiv:1909.01593] [INSPIRE].

[21] J.A. Rubiño Martín et al., *The Tenerife Microwave Spectrometer (TMS) experiment: studying the absolute spectrum of the sky emission in the 10–20GHz range*, in the proceedings of the *Millimeter, Submillimeter, and Far-Infrared Detectors and Instrumentation for Astronomy X*, SPIE (2020) [DOI:10.1117/12.2561309].

[22] P. Alonso-Arias, P.A. Fuerte-Rodríguez, R.J. Hoyland and J.A. Rubiño-Martín, *The optical system of the Tenerife Microwave Spectrometer: a window for observing the 10–20 GHz sky spectra*, 2021 *JINST* **16** P12037 [arXiv:2111.15364] [INSPIRE].

[23] C. Feng and G. Holder, *Enhanced global signal of neutral hydrogen due to excess radiation at cosmic dawn*, *Astrophys. J. Lett.* **858** (2018) L17 [arXiv:1802.07432] [INSPIRE].

[24] S. Furlanetto, S.P. Oh and F. Briggs, *Cosmology at Low Frequencies: The 21 cm Transition and the High-Redshift Universe*, *Phys. Rept.* **433** (2006) 181 [astro-ph/0608032] [INSPIRE].

[25] S.K. Acharya, B. Cyr and J. Chluba, *The role of soft photon injection and heating in 21 cm cosmology*, *Mon. Not. Roy. Astron. Soc.* **523** (2023) 1908 [arXiv:2303.17311] [INSPIRE].

[26] J.D. Bowman et al., *An absorption profile centred at 78 megahertz in the sky-averaged spectrum*, *Nature* **555** (2018) 67 [arXiv:1810.05912] [INSPIRE].

[27] R. Hills, G. Kulkarni, P.D. Meerburg and E. Puchwein, *Concerns about modelling of the EDGES data*, *Nature* **564** (2018) E32 [arXiv:1805.01421] [INSPIRE].

[28] R.F. Bradley, K. Tauscher, D. Rapetti and J.O. Burns, *A Ground Plane Artifact that Induces an Absorption Profile in Averaged Spectra from Global 21-cm Measurements — with Possible Application to EDGES*, *Astrophys. J.* **874** (2019) 153 [arXiv:1810.09015] [INSPIRE].

[29] S. Singh et al., *On the detection of a cosmic dawn signal in the radio background*, *Nature Astron.* **6** (2022) 607 [arXiv:2112.06778] [INSPIRE].

[30] J.D. Bowman et al., *Reply to Hills et al.*, *Nature* **564** (2018) E35.

[31] S.G. Murray et al., *A Bayesian calibration framework for EDGES*, *Mon. Not. Roy. Astron. Soc.* **517** (2022) 2264 [arXiv:2209.03459] [INSPIRE].

[32] H.T.J. Bevins et al., *Astrophysical constraints from the SARAS 3 non-detection of the cosmic dawn sky-averaged 21-cm signal*, *Nature Astron.* **6** (2022) 1473 [arXiv:2212.00464] [INSPIRE].

JCAP04(2024)046

[33] G. Bernardi et al., *Bayesian constraints on the global 21-cm signal from the Cosmic Dawn*, *Mon. Not. Roy. Astron. Soc.* **461** (2016) 2847 [arXiv:1606.06006] [INSPIRE].

[34] J. Singal et al., *The Second Radio Synchrotron Background Workshop: Conference Summary and Report*, *Publ. Astron. Soc. Pac.* **135** (2023) 036001 [arXiv:2211.16547] [INSPIRE].

[35] L. Philip et al., *Probing Radio Intensity at High-Z from Marion: 2017 Instrument*, *J. Astron. Inst.* **08** (2019) 1950004 [arXiv:1806.09531].

[36] E. de Lera Acedo et al., *The REACH radiometer for detecting the 21-cm hydrogen signal from redshift $z \approx 7.5$–28*, *Nature Astron.* **6** (2022) 998 [arXiv:2210.07409] [INSPIRE].

[37] HERA collaboration, *Improved Constraints on the 21 cm EoR Power Spectrum and the X-Ray Heating of the IGM with HERA Phase I Observations*, *Astrophys. J.* **945** (2023) 124 [arXiv:2210.04912] [INSPIRE].

[38] X. Chen et al., *Discovering the Sky at the Longest wavelengths with a lunar orbit array*, *Phil. Trans. Roy. Soc. Lond. A* **379** (2020) 20190566 [arXiv:2007.15794] [INSPIRE].

[39] S.D. Bale et al., *LuSEE 'Night': The Lunar Surface Electromagnetics Experiment*, arXiv:2301.10345.

[40] M. Sathyanarayana Rao et al., *PRATUSH experiment concept and design overview*, *Exper. Astron.* **56** (2023) 741.

[41] R. Barkana, *Possible interaction between baryons and dark-matter particles revealed by the first stars*, *Nature* **555** (2018) 71 [arXiv:1803.06698] [INSPIRE].

[42] J.B. Muñoz and A. Loeb, *A small amount of mini-charged dark matter could cool the baryons in the early Universe*, *Nature* **557** (2018) 684 [arXiv:1802.10094] [INSPIRE].

[43] A. Ewall-Wice et al., *Modeling the Radio Background from the First Black Holes at Cosmic Dawn: Implications for the 21 cm Absorption Amplitude*, *Astrophys. J.* **868** (2018) 63 [arXiv:1803.01815] [INSPIRE].

[44] S. Fraser et al., *The EDGES 21 cm Anomaly and Properties of Dark Matter*, *Phys. Lett. B* **785** (2018) 159 [arXiv:1803.03245] [INSPIRE].

[45] M. Pospelov, J. Pradler, J.T. Ruderman and A. Urbano, *Room for New Physics in the Rayleigh-Jeans Tail of the Cosmic Microwave Background*, *Phys. Rev. Lett.* **121** (2018) 031103 [arXiv:1803.07048] [INSPIRE].

[46] D. Aristizabal Sierra and C.S. Fong, *The EDGES signal: An imprint from the mirror world?*, *Phys. Lett. B* **784** (2018) 130 [arXiv:1805.02685] [INSPIRE].

[47] P. Mertsch et al., *Neutrino clustering in the Milky Way and beyond*, *JCAP* **01** (2020) 015 [arXiv:1910.13388] [INSPIRE].

[48] F. Zimmer, C.A. Correa and S. Ando, *Influence of local structure on relic neutrino abundances and anisotropies*, *JCAP* **11** (2023) 038 [arXiv:2306.16444] [INSPIRE].

[49] E. Masso and R. Toldra, *Photon spectrum produced by the late decay of a cosmic neutrino background*, *Phys. Rev. D* **60** (1999) 083503 [astro-ph/9903397] [INSPIRE].

[50] PLANCK collaboration, *Planck 2018 results. VI. Cosmological parameters*, *Astron. Astrophys.* **641** (2020) A6 [*Erratum ibid.* **652** (2021) C4] [arXiv:1807.06209] [INSPIRE].

[51] Y.S. Murakami et al., *Leveraging SN Ia spectroscopic similarity to improve the measurement of $H_0$*, *JCAP* **11** (2023) 046 [arXiv:2306.00070] [INSPIRE].



JCAP04(2024)046

[52] P. Di Bari, *Cosmology and the early Universe*, Series in Astronomy and Astrophysics, CRC Press (2018).

[53] J.R. Pritchard and A. Loeb, *21-cm cosmology*, *Rept. Prog. Phys.* **75** (2012) 086901 [arXiv:1109.6012] [INSPIRE].

[54] M. Zaldarriaga, S.R. Furlanetto and L. Hernquist, *21 Centimeter fluctuations from cosmic gas at high redshifts*, *Astrophys. J.* **608** (2004) 622 [astro-ph/0311514] [INSPIRE].

[55] A. Fialkov and R. Barkana, *Signature of Excess Radio Background in the 21-cm Global Signal and Power Spectrum*, *Mon. Not. Roy. Astron. Soc.* **486** (2019) 1763 [arXiv:1902.02438] [INSPIRE].

[56] R. Subrahmanyan et al., *An Australia telescope survey for CMB anisotropies*, *Mon. Not. Roy. Astron. Soc.* **315** (2000) 808 [astro-ph/0002467] [INSPIRE].

[57] B. Bolliet, J. Chluba and R. Battye, *Spectral distortion constraints on photon injection from low-mass decaying particles*, *Mon. Not. Roy. Astron. Soc.* **507** (2021) 3148 [arXiv:2012.07292] [INSPIRE].

[58] B. Dev, P. Di Bari, I. Martínez-Soler and R. Roshan, in preparation.

[59] K.S. Babu, X.-G. He, M. Su and A. Thapa, *Naturally light Dirac and pseudo-Dirac neutrinos from left-right symmetry*, *JHEP* **08** (2022) 140 [arXiv:2205.09127] [INSPIRE].

[60] K. Carloni et al., *Probing Pseudo-Dirac Neutrinos with Astrophysical Sources at IceCube*, arXiv:2212.00737 [INSPIRE].

[61] H. Ooguri and C. Vafa, *Non-supersymmetric AdS and the Swampland*, *Adv. Theor. Math. Phys.* **21** (2017) 1787 [arXiv:1610.01533] [INSPIRE].

[62] L.E. Ibáñez, V. Martín-Lozano and I. Valenzuela, *Constraining Neutrino Masses, the Cosmological Constant and BSM Physics from the Weak Gravity Conjecture*, *JHEP* **11** (2017) 066 [arXiv:1706.05392] [INSPIRE].

[63] E. Gonzalo, L.E. Ibáñez and I. Valenzuela, *Swampland constraints on neutrino masses*, *JHEP* **02** (2022) 088 [arXiv:2109.10961] [INSPIRE].

[64] A. de Gouvea, W.-C. Huang and J. Jenkins, *Pseudo-Dirac Neutrinos in the New Standard Model*, *Phys. Rev. D* **80** (2009) 073007 [arXiv:0906.1611] [INSPIRE].

[65] S. Ansarifard and Y. Farzan, *Revisiting pseudo-Dirac neutrino scenario after recent solar neutrino data*, *Phys. Rev. D* **107** (2023) 075029 [arXiv:2211.09105] [INSPIRE].

[66] Z. Chen, J. Liao, J. Ling and B. Yue, *Constraining super-light sterile neutrinos at Borexino and KamLAND*, *JHEP* **09** (2022) 004 [arXiv:2205.07574] [INSPIRE].

[67] J. Franklin, Y.F. Perez-González and J. Turner, *JUNO as a probe of the pseudo-Dirac nature using solar neutrinos*, *Phys. Rev. D* **108** (2023) 035010 [arXiv:2304.05418] [INSPIRE].

[68] R.M. Crocker, F. Melia and R.R. Volkas, *Searching for long wavelength neutrino oscillations in the distorted neutrino spectrum of galactic supernova remnants*, *Astrophys. J. Suppl.* **141** (2002) 147 [astro-ph/0106090] [INSPIRE].

[69] R.M. Crocker, F. Melia and R.R. Volkas, *Oscillating neutrinos from the galactic center*, *Astrophys. J. Suppl.* **130** (2000) 339 [astro-ph/9911292] [INSPIRE].

[70] P. Keranen, J. Maalampi, M. Myyrylainen and J. Riittinen, *Effects of sterile neutrinos on the ultrahigh-energy cosmic neutrino flux*, *Phys. Lett. B* **574** (2003) 162 [hep-ph/0307041] [INSPIRE].

JCAP04(2024)046

[71] J.F. Beacom et al., *PseudoDirac neutrinos: A challenge for neutrino telescopes*, *Phys. Rev. Lett.* **92** (2004) 011101 [hep-ph/0307151] [INSPIRE].

[72] A. Esmaili, *Pseudo-Dirac Neutrino Scenario: Cosmic Neutrinos at Neutrino Telescopes*, *Phys. Rev. D* **81** (2010) 013006 [arXiv:0909.5410] [INSPIRE].

[73] A. Esmaili and Y. Farzan, *Implications of the Pseudo-Dirac Scenario for Ultra High Energy Neutrinos from GRBs*, *JCAP* **12** (2012) 014 [arXiv:1208.6012] [INSPIRE].

[74] I. Martínez-Soler, Y.F. Perez-González and M. Sen, *Signs of pseudo-Dirac neutrinos in SN1987A data*, *Phys. Rev. D* **105** (2022) 095019 [arXiv:2105.12736] [INSPIRE].

[75] T. Rink and M. Sen, *Constraints on pseudo-Dirac neutrinos using high-energy neutrinos from NGC 1068*, *Phys. Lett. B* **851** (2024) 138558 [arXiv:2211.16520] [INSPIRE].

JCAP04(2024)046